Disruption and Formation of Surface Salt Bridges Are Coupled to DNA Binding by the Integration Host Factor: A Computational Analysis

ARTICLE *in* BIOCHEMISTRY · DECEMBER 2010

Impact Factor: 3.02 · DOI: 10.1021/bi101096k · Source: PubMed

4 AUTHORS, INCLUDING:

Qiang Cui
University of Wisconsin–Madison
201 PUBLICATIONS **13,464** CITATIONS

266 *Biochemistry* **2011,** *50,* 266–275
DOI: 10.1021/bi101096k

BIOCHEMISTRY
including biophysical chemistry & molecular biology
Article

Disruption and Formation of Surface Salt Bridges Are Coupled to DNA Binding by the Integration Host Factor: A Computational Analysis[†]

L. Ma,[‡,@] N. K. Sundlass,[‡,§,@] R. T. Raines,[∥,⊥] and Q. Cui*[,⊥]

[‡]*Graduate Program in Biophysics,* [§]*Medical Scientist Training Program, and* [∥]*Department of Biochemistry, University of Wisconsin, 433 Babcock Drive, Madison, Wisconsin 53706, United States, and* [⊥]*Department of Chemistry, University of Wisconsin, 1101 University Avenue, Madison, Wisconsin 53706, United States.* [@]*These authors contributed equally to this work.*

Received July 9, 2010; Revised Manuscript Received November 30, 2010

ABSTRACT: Revealing the thermodynamic driving force of protein−DNA interactions is crucial to the understanding of factors that dictate the properties and function of protein−DNA complexes. For the binding of DNA to DNA-wrapping proteins, such as the integration host factor (IHF), Record and co-workers proposed that the disruption of a large number of preexisting salt bridges is coupled with the binding process [Holbrook, J. A., et al. (2001) *J. Mol. Biol. 310*, 379]. To test this proposal, we have conducted explicit solvent MD simulations (multiple ∼25−50 ns trajectories for each salt concentration) to examine the behavior of charged residues in IHF, especially concerning their ability to form salt bridges at different salt concentrations. Of the 17 cationic residues noted by Record and co-workers, most are engaged in salt bridge interactions for a significant portion of the trajectories, especially in the absence of salt. This observation suggests that, from a structural point of view, their proposal is plausible. However, the complex behaviors of charged residues observed in the MD simulations also suggest that the unusual thermodynamic characteristics of IHF−DNA binding likely arise from the interplay between complex dynamics of charged residues both in and beyond the DNA binding site. Moreover, a comparison of MD simulations at different salt concentrations suggests that the strong dependence of the IHF−DNA binding enthalpy on salt concentration may not be due to a significant decrease in the number of stable salt bridges in apo IHF at high salt concentrations. In addition to the Hofmeister effects quantified in more recent studies of IHF−DNA binding, we recommend consideration of the variation of the enthalpy change of salt bridge disruption at different salt concentrations. Finally, the simulation study presented here explicitly highlights the fact that the electrostatic properties of DNA-binding proteins can be rather different in the apo and DNA-bound states, which has important implications for the design of robust methods for predicting DNA binding sites in proteins.

Protein−DNA complexes play multiple important roles in cellular processes that involve DNA "transactions", such as replication, transcription, recombination, and repair as well as the packaging of chromosomal DNA (*1*). Proteins that interact with DNA in these complexes either serve as enzymes [e.g., DNA polymerase (*2*)] to catalyze biochemical reactions or simply act as an "architectural scaffold" (*3*) to manipulate the structure of DNA by, for example, bending and/or wrapping DNA. Well-known examples in the latter category include IHF[1] (*4*, *5*) and HU (*5*). Because of significant structural deviation from the equilibrium form of DNA (most often from the B-form), the mechanical work associated with DNA bending and/or wrapping needs to be compensated by the free energy gain of protein−DNA binding (*6*, *7*). Therefore, it is important to understand the thermodynamic driving force of protein−DNA binding, especially for architectural scaffolding proteins.

IHF is a remarkable example of a DNA-bending/wrapping protein (*4*, *5*). It bends the specific 34 bp DNA segment by as much as ∼160°, as illustrated by the crystal structure of an IHF−DNA complex (*8*) (see Figure 1a). To investigate the mechanism of IHF−DNA binding, Record and co-workers (*9*) explored extensively the thermodynamics of specific and non-specific interactions between IHF and DNA using isothermal titration calorimetry. These experiments revealed several unusual thermodynamic features of IHF−DNA interactions. (i) The binding is highly exothermic and strongly enthalpy-driven while being entropically unfavorable. (ii) The measured salt concentration dependence of the binding constant, SK_{obs}, is much smaller in magnitude than that estimated on the basis of the oligocation model of the binding interface. (iii) The enthalpy change ΔH°_{sp} and heat capacity change ΔC°_{sp} of the specific binding are strongly dependent on the salt concentration ([KCl]), and their magnitudes decrease significantly with increasing [KCl] between 100 and 350 mM.

To rationalize these unexpected features, Record and co-workers (*9*) proposed that IHF−DNA binding is coupled with the disruption of a large number of salt bridges that exist in the unbound form of IHF. In the crystal structure for the IHF−DNA complex (*8*), there are 23 cationic residues located within 6 Å of DNA phosphoryl groups (*9*). This number is significantly

[†]The research was supported by National Institutes of Health Grants R01-GM071428 to Q.C. and R01-CA073808 to R.T.R.

*To whom correspondence should be addressed. E-mail: cui@chem.wisc.edu. Phone: (608) 262-9801. Fax: (608) 262-9918.

[1]Abbreviations: HU, histone-like protein from *Escherichia coli* strain U93; IHF, integration host factor; MD, molecular dynamics; PB, Poisson−Boltzmann; PDB, Protein Data Bank; rmsd and rmsf, root-mean-square difference and fluctuation, respectively.

 Published on Web 12/02/2010

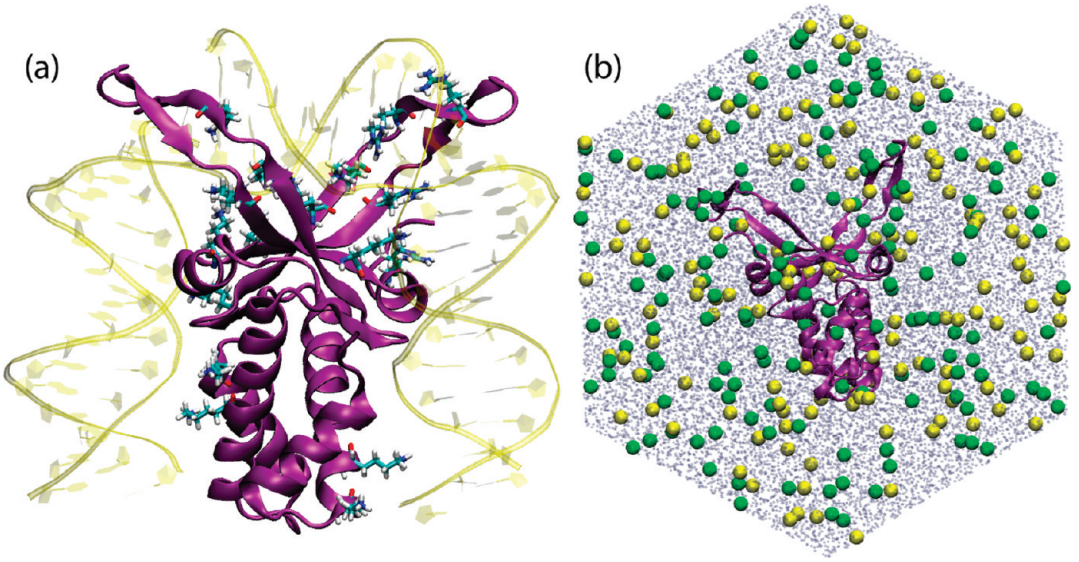

FIGURE 1: Structure of IHF. (a) Crystal structure of the IHF−DNA complex [PDB entry 1IHF (*8*)]. IHF is shown as a purple cartoon, while DNA is shown as yellow ribbons. The 17 cationic residues proposed by Record and co-workers (not including two His residues, H54 and H79) are shown as licorice. (b) Snapshot from MD simulations of apo IHF at 350 mM KCl. The starting structure was obtained from the crystal structure of the IHF−DNA complex [PDB entry 1IHF (*8*)], from which the DNA was removed. IHF is shown as a purple cartoon. Oxygen atoms of water molecules are shown as ice blue points. K^+ and Cl^- ions are shown as yellow and green spheres, respectively. This figure was made using VMD (*48*).

larger than the average value (~12) found on the basis of a large database of protein−DNA complexes (*10*). Interestingly, there are also many anionic residues near these cationic residues. On the basis of an analysis of the position of these charged residues, Record and co-workers (*9*) suggested that 19 of these 23 cationic residues can form salt bridges with nearby anionic residues following either side chain rotations or backbone movements of flexible regions in the protein. Accordingly, they proposed that these salt bridges exist in the unbound form of IHF and are disrupted upon DNA binding and that disruption of salt bridges is the origin of the unusual thermodynamic features of the binding process. For example, the enthalpy change for salt bridge disruption is known to be negative (*11*), which explains the large exothermicity (enthalpic change) of the overall IHF−DNA binding process. They also proposed that the salt bridges become unstable at high K^+ concentrations presumably because of the screening effect of salt ions; the disruption of a reduced number of salt bridges during binding then decreases the magnitude of the enthalpy change at high K^+ concentrations, which was observed experimentally. Moreover, in a recent review (*12*), Saecker and Record further speculated that the disruption of surface salt bridges coupled to DNA binding may not be unique to IHF and may occur in other DNA-wrapping proteins as well, highlighting the possible generality of this phenomenon and its potential role in regulating DNA wrapping. Recent studies of Grove and co-workers (*13*, *14*) have pointed to the potential involvement of surface salt bridges in the determination of the length of the DNA binding site in HU.

Because the proposal of salt bridge disruption was based on a structural analysis of the IHF−DNA complex, one may argue that the evidence is indirect without a high-resolution structure for IHF in the unbound state. For example, considering the small free energy gain associated with salt bridge formation at the protein surface (*15*, *16*), it is not clear if a large number (~23) of surface salt bridges would exist in the unbound state of IHF. Moreover, the simulation study of Elcock and co-workers (*17*) found that the stability of salt bridges is only marginally perturbed by a salt concentration of up to 2 M; thus, the observed KCl concentration dependence of IHF−DNA binding thermodynamics in experiments (*9*) may not be due to perturbations in the number of stable salt bridges. Indeed, more recent analysis by Vander Meulen et al. (*18*) that compared binding thermodynamics of the IHF−DNA complex in different salt solutions (KCl, KF, and KGlu) indicated that the strong salt dependence of the binding enthalpy is a Hofmeister effect arising from interaction of Cl^- with the surfaces buried during binding. Nevertheless, the extrapolated binding enthalpy at low salt concentrations is still highly negative, which is consistent with the salt bridge disruption model.

These considerations have stimulated us to conduct molecular dynamics simulations to investigate salt bridge dynamics in IHF (see Figure 1b for snapshots). Considering the size of the system and complexity of the DNA binding process, we do not anticipate a quantitative comparison with experiments. The goal of the study is to explore whether the salt bridges proposed by Record and co-workers (*9*) are able to form and remain stable when IHF is not interacting with DNA. Along this line, we note that IHF has a large number of charged residues (36 cationic and 28 anionic residues of 190 residues in total); thus, it is interesting to investigate whether the salt bridges near the DNA binding site behave differently compared to other charged residues. In addition, we seek to investigate whether the propensity of salt bridge formation is perturbed by the presence of salt (K^+). Finally, because salt bridge formation and disruption are expected to significantly perturb electrostatic properties, which are used in many algorithms aimed at predicting DNA binding sites in proteins, it is of great interest to explore how sampling salt bridge dynamics impacts such predictions.

COMPUTATIONAL METHODS

Molecular Dynamics Simulations of IHF in the Unbound State. Because the structure of the apo form of IHF is not available, we generated a model by simply removing DNA from

the crystal structure of the IHF−DNA complex [PDB entry 1IHF (*8*)]. Starting from this structure, MD simulations were conducted at two KCl concentrations: 0 mM (termed "no-salt") and 350 mM (termed "high-salt"); 350 mM was chosen because it was the highest salt concentration investigated in the experiments of Record and co-workers (*9*). The simulations were performed using GROMACS (*19*, *20*) with the OPLS-AA force field (*21*) for IHF and ions. To set up the simulation, IHF was first solvated with a rhombic dodecahedron solvent box of TIP4P water (*22*) ($a = b = c = 100$ Å). The TIP4P water model was adopted because of its compatibility with the OPLS-AA force field. K^+ and Cl^- ions were then added into the simulation box according to the proper salt concentration. Because IHF bears a net charge of +8, eight Cl^- ions were added in the no-salt system, and 149 K^+ and 157 Cl^- ions in the high-salt system, to achieve overall charge neutrality; snapshots of the two systems are shown in Figure 1. The periodic boundary condition was applied, and long-range electrostatics were treated with the particle mesh Ewald method (*23*). For van der Waals interactions, a switching cutoff scheme (*24*) for interatomic distances between 10 and 12 Å was used. The SETTLE (*25*) (for water) and SHAKE (*26*) (for protein) algorithms were applied to constrain bonds involving hydrogen atoms to allow an integration time step of 2 fs. The systems were equilibrated for 1 ns at 300 K with the NVT ensemble, which was followed by 25−50 ns production runs with the NPT ensemble; three independent trajectories were conducted for each salt concentration. Temperature was controlled using the Nose−Hoover scheme (*27*, *28*), and pressure was controlled with the Berendsen scheme (*29*). Considering the large number of charged residues in IHF (36 cationic and 28 anionic), we expected that three independent 25−50 ns trajectories were sufficient for observing statistically meaningful behaviors of salt bridges (see Figure 4 and the Supporting Information).

Because the system has many titratable residues, it is of interest to question whether many residues adopt an unexpected protonation state. Considering the fairly large conformational changes during the simulation, we did not pursue computationally intensive pK_a analysis such as with MCCE (*30*); this was in part justified by the observation that most titratable residues are solvent accessible and therefore not expected to have very large pK_a shifts. This was confirmed by running pK_a calculations with the empirical PROPKA approach (*31*, *32*) with several different snapshots from the MD simulations; all Glu/Asp residues were predicted to be deprotonated and Lys/Arg residues protonated. Along the same line, our work addresses salt bridge interactions involving residues that are largely solvated rather than buried in the protein interior; thus, the lack of explicit polarization in the force field is unlikely a serious issue. Recent analysis highlights the fact that including polarization is most essential in problems that involve polar−nonpolar interfaces (*33*−*35*).

Calculations of Protein Surface Electrostatic Potential. To compare the electrostatic properties of IHF in different structures, we performed linear PB calculations. Calculations were conducted using the PBEQ module in CHARMM (*36*), and the molecular surface was adopted to define the dielectric boundary between protein and solvent. Specifically, the set of atomic radii developed by Roux and co-workers (*37*) was used together with a solvent probe radius of 1.4 Å and an ion exclusion layer of 2 Å. The partial charges for protein atoms were adopted from the standard CHARMM 27 force field (*38*). The multigrid setup was used to solve PB numerically, and the focusing scheme was applied: coarser grid of 160 Å × 160 Å × 160 Å with a 1.0 Å spacing and finer grid of 82 Å × 68 Å × 64 Å with a 0.4 Å spacing. The salt concentration was set as the physiological concentration of 0.15 M, and the dielectric constant was set to 2 and 80 for the protein and water, respectively. The electrostatic potential ϕ_i was first calculated for each grid point i in the finer grid enclosing the protein; the values were then used to compute residue-averaged electrostatic potential (ϕ^j_{res}) using the PBAV option in CHARMM (*36*). Specifically, ϕ^j_{res} is the average of ϕ_i over all grid points i that belong to residue j (within the van der Waals radii of all atoms of residue j):

$$\phi^j_{res} = \frac{1}{N_j}\sum_{i,\, i\in j}^{N_j} \phi_i \qquad (1)$$

where N_j is the number of grid points that belong to residue j.

Prediction of the DNA Binding Interface. To investigate how a change in electrostatic potentials (because of salt bridge rearrangements) impacts the prediction of the DNA binding site (see Impact on the Prediction of DNA Binding Sites for a detailed discussions), we select two popular web servers that predict DNA binding interfaces in proteins. The first one is patch plus finder (PPF) (*39*) (http://pfp.technion.ac.il/), which finds the largest continuous patch on the protein surface that has positive electrostatic potential. The second one is Preds (*40*, *41*) (http://pre-s.protein.osaka-u.ac.jp/preds/), which predicts whether a protein is capable of binding DNA and, if so, the location of the binding interface. The prediction is characterized by a statistical score, P_{score}, which is calculated mainly on the basis of the surface electrostatic potential and the molecular shape of the protein. The only required input for both web severs is the protein structure in the standard PDB format.

RESULTS AND DISCUSSION

Although three independent trajectories were calculated for each salt concentration, the results are qualitatively similar. Therefore, in the following discussions, unless explicitly stated, results for the longest simulation (50 ns) are discussed.

Overall Conformational Stability of IHF in the Absence of DNA. Without the DNA, it is expected that the structure of IHF undergoes relaxation away from its conformation in the IHF−DNA complex (which is the starting configuration of the MD simulations). IHF is a heterodimer with two subunits, α and β, and can be divided into two domains according to secondary structure content and functional roles. The first domain (residues excluding residues 54−77 on both subunits, colored green in Figure 2a) is made up mainly of α helices and is named the core domain; the second "arm" domain (residues 54−77 on both subunits, colored yellow in Figure 2a), on the other hand, consists mainly of β sheets and embraces the bound DNA in the IHF−DNA complex. As shown in Figure 2a, the core domain is relatively stable and the arm domain has more significant conformational changes during the MD simulations. To analyze the structural transitions more quantitatively, the rmsd values of the backbone non-hydrogen atoms in the two domains were calculated along MD trajectories relative to the starting structure; the backbone non-hydrogen atoms of the core domain were used as the reference for the best fit in the rmsd calculations. As shown in Figure 2b, the rmsd of the core domain is ~2 Å throughout the 50 ns simulations under both no-salt (0 mM KCl) and high-salt (350 mM KCl) conditions, which indicates that the core domain remains stable in the absence of DNA. The rmsd of the arm

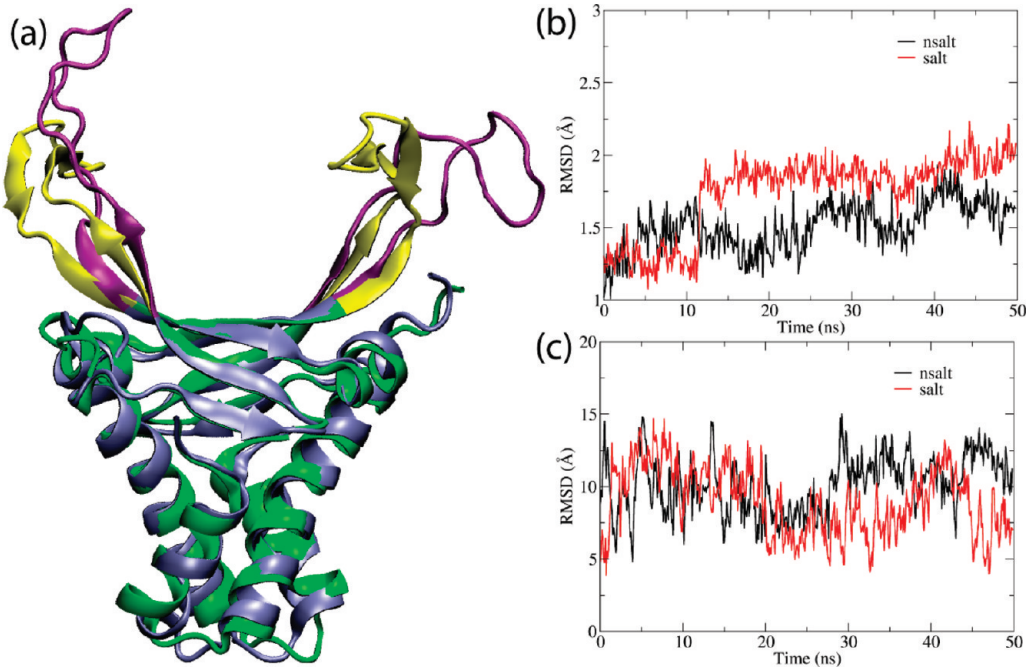

FIGURE 2: Conformational transitions in IHF observed within 50 ns MD simulations (results for other two independent 25 ns simulations for each salt concentration are qualitatively similar and therefore not shown). (a) Overlap of IHF conformation in the IHF−DNA complex [PDB entry 1IHF (*8*)] and a random snapshot by the end of the no-salt MD simulation. The backbone atoms of the core domain were used as the best-fit region. The core and arm domains of the crystal conformation are colored green and yellow, respectively, while those in the MD snapshot are colored gray and purple, respectively. (b and c) rmsd values of backbone atoms of (b) the core domain and (c) the arm domain along MD trajectories with respect to the crystal conformation of IHF with the backbone atoms of the core domain as the best-fit region.

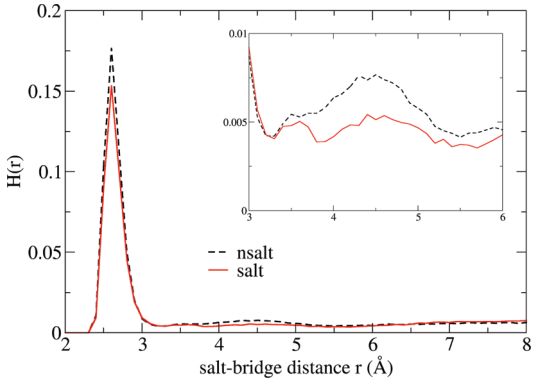

FIGURE 3: Normalized histogram $H(r)$ of salt bridge distance r_{min-NO} (the minimal distance between N in a cationic residue and O in all anionic residues) for all 36 cationic residues collected from no-salt and high-salt simulations. The inset shows the small peak between 3 and 6 Å.

domain, however, can be as large as ~10 Å in both sets of trajectories, suggesting that the arm domain, which embraces DNA in the complex, becomes very floppy after DNA is removed. Moreover, the β-sheet structure in the arm domain (colored purple in Figure 2a) undergoes partial unfolding during simulations, which hints at the possibility that IHF−DNA binding is coupled with a local folding transition in the arm domain, which is often observed in the formation of specific protein−DNA complexes (*42*).

Salt Bridge Dynamics. In the proposal by Record and coworkers (*9*), 19 of the 23 cationic residues in the DNA binding interface have the potential to (re)form salt bridges with nearby anionic residues in the absence of DNA. The potential salt bridge partners for two His residues (H54 and H79) on the β subunit are two anionic residues (D98 and D99) near the C-terminius of the α subunit, which is missing in the crystal structure of the IHF−DNA complex and therefore not included in our simulation. Thus, these two His residues are not included in the subsequent analysis, and we focus on the 17 remaining cationic residues (all are Lys or Arg); they are termed the 17 binding-site cationic residues. Moreover, as mentioned in the introductory section, there are in total 36 cationic residues in IHF; thus, we also explore the behaviors of the 19 remaining cationic residue in terms of the formation of salt bridge interactions.

(*i*) *Distribution of Salt Bridge Distances*. To analyze the propensity of all 36 cationic residues for forming salt bridge interactions, we first monitor the shortest distance between the nitrogen atoms of each cationic residue and the oxygen atoms in all anionic residues (r_{min-NO}); as examples, the detailed data for all 36 cationic residues during the 50 ns trajectories are included as Supporting Information. To establish a distance criterion for defining salt bridge formation, a classical statistical study (*43*) concluded that an r_{min-NO} of ≤4 Å should be used because this criterion leads to the largest difference in the frequency of observing oppositely charged pairs versus likely charged pairs in protein crystal structures. In the analysis of Record and coworkers (*9*), however, an r_{min-NO} of ≤3 Å was used instead as a criterion for dehydrated (i.e., no solvent between) salt bridges. To determine which criterion is more appropriate for this study, we calculated the normalized histogram, $H(r_{min-NO})$, for all 36 cationic residues collected from both no-salt and high-salt simulations; the volume factor $4\pi r_{min-NO}^2$ is not included for the sake of simplicity. As shown in Figure 3, there is a large and sharp peak between 2 and 3.5 Å, which corresponds to the dehydrated salt bridge state, and another small peak (shown in the inset of Figure 3) between 3.5 and 5.5 Å, which corresponds to the solvent-mediated ion pair. In a recent computational study (*17*) of acetate−methylammonium (model compounds

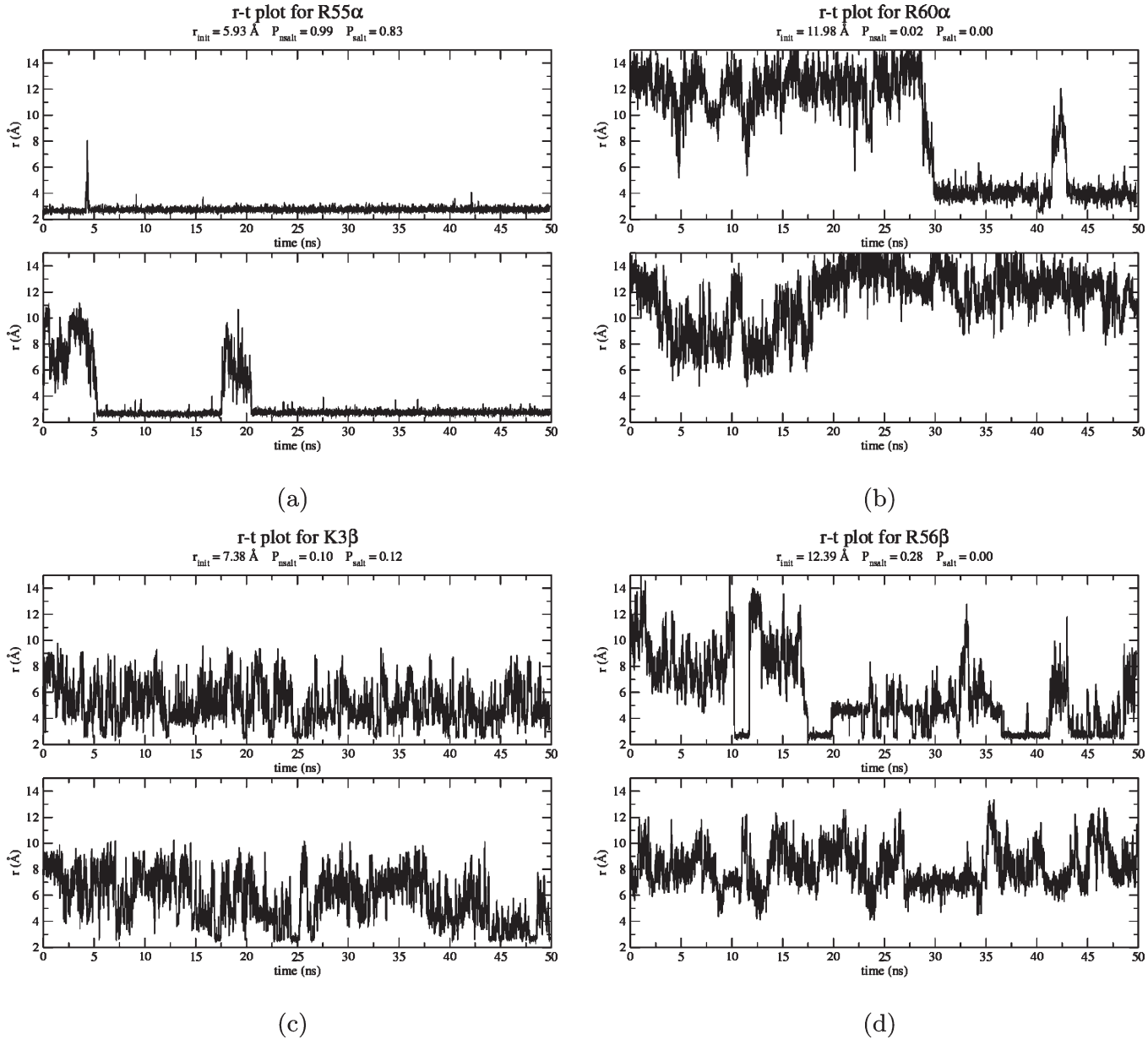

FIGURE 4: Representative behaviors of salt bridges involving binding-site cationic residues during MD simulations with no-salt (0 M KCl, top panel for each residue) and high-salt (350 mM KCl, bottom panel for each residue) conditions; results for two other independent 25 ns simulations for each salt concentration are qualitatively similar and therefore not shown. The salt bridge distance r for a specific cationic residue is the minimal distance between its side chain N atom and side chain O atoms in all anionic residues; r_{init} indicates the value in the crystal structure. For the behaviors of other cationic residues (both in and beyond the DNA binding site), see the Supporting Information.

for salt bridges) association, three minima were observed in the potential of mean force: one for the direct (dehydrated) interaction and two others for solvent-separated interactions. The positions of the first two minima in that work are essentially the same as those found here. The boundary between the two peaks in Figure 3 falls around 3.3 Å; therefore, the distance criterion for defining a dehydrated salt bridge is chosen as $r_{min-NO} \leq 3.3$ Å, which is used in all subsequent analysis. This criterion is similar to that used by Record and co-workers (*9*) while more strict than that from the statistical study (*43*). Comparison between the no-salt and high-salt results in Figure 3 suggests that an increasing salt concentration decreases the probability of forming dehydrated salt bridges (the first peak) and the solvent-mediated ion pair (the second peak); as discussed in more detail below, however, the magnitude of the effect is rather small.

(*ii*) *Salt Bridge Formation for the 17 Binding-Site Cationic Residues in the Absence of KCl.* As shown in Figure 4 and figures in the Supporting Information, there is complex behavior in the salt bridge dynamics. The salt bridge formation probability P for a specific cationic residue is defined as the fraction of simulation time during which this residue is engaged in a salt bridge interaction as determined on the basis of the $r_{min-NO} \leq 3.3$ Å criterion. Although we have conducted only three 25−50 ns trajectories for each salt concentration, there are significant fluctuations in the salt bridge distances during the simulations for most cationic residues; thus, the overall trends in P are expected to be meaningful. For example, the qualitative behaviors of the salt bridges are fairly similar among the three independent trajectories. As shown in Table 1, P varies rather significantly between 0 and 1 for the 17 binding-site cationic residues discussed by Record and co-workers (*9*). Nevertheless, the majority of these

residues have formed salt bridges within 25−50 ns with considerable P values; this is true especially in the no-salt simulation. For example, if we (arbitrarily) choose a $P = 0.1$ cutoff, 12 of the 17 binding-site cationic residues form salt bridges in the no-salt simulation. This is quite remarkable because some of the cationic residues are rather far from any anionic residue in the starting (IHF−DNA complex) structure; the most striking example is R56β, which is 12.4 Å from any anionic residue in the initial structure but has a significant P value of ~0.3 in three independent trajectories (also see Figure 4d). Some salt bridges form quickly and remain stable throughout the simulation; for example, K20α, R55α (Figure 4a), K75β, and R87β all have P values higher than 0.90 in at least one of the three independent trajectories. Of the 17 binding-site cationic residues, five of them (K45α, K57α, R60α, R59β, and K81β) do not lead to significant salt bridge formation ($P < 0.01$) during any of the 25−50 ns simulations, and they are all rather far from anionic residues in the initial structure ($r_{min-NO} < 7.5$ Å); thus, salt bridge formation likely implicates structural transitions at longer time scales (for their location in IHF, see Figure 5b). Nevertheless, even some of these residues come rather close to forming stable salt bridges during the simulations (e.g., see Figure 4b for R60α, for which r_{min-NO} decreases from ~14 to ~4 Å). In short, the simulations clearly illustrate that, in the absence of salt, a majority of the cationic residues in the DNA binding region have significant propensity to form salt bridges in the absence of DNA.

Table 1: r_{init}, $P_{no\text{-}salt}$, and P_{salt} Values for the 17 Binding-Site Cationic Residues[a]

residue	r_{init} (Å)	$P_{no\text{-}salt}$	P_{salt}	residue	r_{init} (Å)	$P_{no\text{-}salt}$	P_{salt}
K20α	3.9	0.99	0.95	K3β	7.4	0.10	0.12
		0.96/0.97	0.98/0.97			0.19/0.13	0.07/0.00
K24α	7.0	0.22	0.31	K27β	3.7	0.80	0.42
		0.05/0.14	0.16/0.00			0.86/0.59	0.53/0.61
K45α	7.6	0.00	0.00	**R56β**	**12.4**	**0.28**	**0.00**
		0.00/0.00	0.00/0.00			**0.33/0.32**	**0.00/0.00**
R55α	5.9	0.99	0.83	R59β	9.3	0.00	0.00
		0.89/0.83	0.63/0.03			0.00/0.02	0.00/0.00
K57α	10.0	0.00	0.00	K75β	5.2	0.60	0.89
		0.00/0.00	0.00/0.00			0.95/0.65	0.89/0.87
R60α	12.0	0.02	0.00	K81β	9.5	0.00	0.00
		0.00/0.00	0.00/0.00			0.00/0.00	0.00/0.00
R63α	4.4	0.42	0.68	**R87β**	**5.9**	**0.90**	**0.00**
		0.38/0.93	0.90/0.66			**0.55/0.99**	**0.00/0.00**
R76α	**6.6**	**0.77**	**0.00**				
		0.01/0.00	0.00/0.00				
R82α	4.4	0.63	0.70				
		0.57/0.60	0.70/0.75				
K88α	**9.3**	**0.55**	**0.00**				
		0.03/0.16	0.00/0.00				

[a] r_{init} (in angstroms) is the minimal distance between N in a cationic residue and O in all anionic residues in IHF in the IHF−DNA complex [PDB entry 1IHF (*8*)]. $P_{no\text{-}salt}$ and P_{salt} are the probabilities of salt bridge formation in no-salt and high-salt simulations, respectively. Residues shown in bold exhibit the most significant difference between $P_{no\text{-}salt}$ and P_{salt} (also shown as circled red dots in Figure 5). For each residue, the first row gives the value from a 50 ns simulation while the second row gives the value from two other independent 25 ns simulations.

(*iii*) *Salt Bridge Dynamics for the 19 Other Cationic Residues*. Among 19 other cationic residues, which are farther from the DNA binding site in the IHF−DNA complex structure, 11 of them are engaged in salt bridge interactions in the IHF−DNA complex (i.e., $r_{min\text{-}NO} < 3.3$ Å); all these, except K20β (see below), have high P values throughout the simulation. Among the rest, five of them (K15α, R21α, R77α, K97α, and K69β) also have significant P values (Table 2), although they are not engaged in salt bridges in the IHF−DNA complex. Therefore, this simulation suggests that the disruption of salt bridges involving these cationic residues may also be coupled to the DNA binding process and contribute to the unusual thermodynamic features of IHF−DNA binding. These residues were not considered by Record and co-workers because they are more than 6 Å from the phosphoryl oxygen atoms of DNA in the crystal complex structure (*8*). Because electrostatic interactions are relatively long-range, it is not unreasonable that DNA binding can perturb interactions beyond the immediate binding region. On the other hand, to firmly support the involvement of these

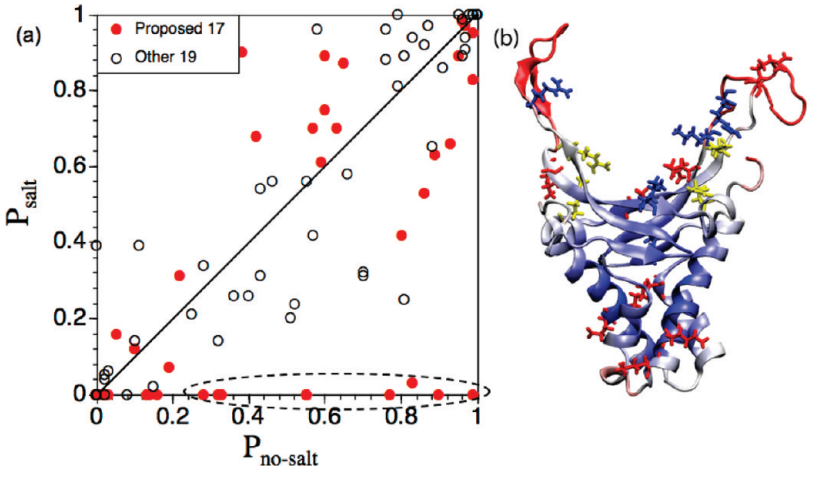

FIGURE 5: Behavior of cationic residues in IHF during MD simulations. (a) Correlation between $P_{no\text{-}salt}$ and P_{salt} for all 36 cationic residues. The 17 binding-site cationic residues are shown as red dots, while the other 19 are shown as empty circles; for each residue, results for three independent pairs of simulations are shown as separate data points. The circled red dots indicate four residues that exhibit the most signifiant differences between $P_{no\text{-}salt}$ and P_{salt} (also see Table 1). The $P_{no\text{-}salt} = P_{salt}$ line is meant to guide the eye. (b) Random snapshot from the no-salt simulation. IHF is shown as a cartoon colored according to the rmsf (red, high rmsf; blue, low rmsf). The 17 binding-site cationic residues are shown as licorice in different colors according to their salt bridge formation probabilities: residues whose $P_{no\text{-}salt}$ and P_{salt} are both greater than 0.10 are colored red; residues whose $P_{no\text{-}salt}$ and P_{salt} are both lower than 0.10 are colored blue; residues with high $P_{no\text{-}salt}$ but low P_{salt} (bold in Table 1 and circled in panel a) are colored yellow.

cationic residues, one needs to verify that these cationic residues do not engage in salt bridge interactions in an MD simulation of the IHF−DNA complex, which is beyond the scope of this work.

As mentioned above, K20β is somewhat unusual in that it forms salt bridges in the IHF−DNA complex structure but these salt bridges become completely disrupted in the absence of DNA in all three independent trajectories (see Table 2 and the Supporting Information). This behavior is strikingly different from that of the 35 other cationic residues and motivates further structural analysis of this residue. The local environment of K20β at different stages of the simulation is shown in Figure 6: in the initial structure, K20β forms bifurcated salt bridges with E23β and D24β; in the absence of DNA, as shown by a snapshot at 22.4 ns in the no-salt simulation (high-salt simulation shows similar behavior) in Figure 6b, these two salt bridges are broken and E23β and D24β form salt bridges with two of the 17 binding-site cationic residues, K3β and K27β. Therefore, in addition to the disruption of salt bridges, there is also salt bridge switching (coupled disruption and formation) involved in the DNA binding process.

(*iv*) *Effects of KCl Concentration on Salt Bridge Formation*. To explore the effect of KCl on salt bridge formation, we compare P for all 36 cationic residues under no-salt and high-salt conditions; because only three trajectories are run for each salt concentration, we show the P values from these simulations as separate data points in Figure 5a rather than attempting to compute standard deviations. As shown in Figure 5a, for most residues the effect of KCl concentration is rather minor (also see panels a and c of Figure 4 for R55α and K3β, respectively, as representative examples). The exception is for four cationic residues in the DNA binding region: R76α, K88α, R56β, and R87β. These four residues (shown in bold in Table 1 and in yellow in Figure 5b) have considerable P values under no-salt conditions but essentially a zero P value with 350 mM KCl. A common feature of these four residues is that they are relatively far from anionic residues in the starting structure (see the Supporting Information for details); the shortest $r_{\text{min-NO}}$ is for R87β, which is 5.9 Å. As shown in Figure 4d for R56β, although $r_{\text{min-NO}}$ is seen to decrease substantially from the initial (crystal) value of 12.4 Å to the salt bridge range (≤3.3 Å) in the no-salt simulation, the distance rarely decreases to <5 Å in the high-salt simulation. Therefore, the overall trend is that KCl has a significant impact on salt bridge formation only if the charged residues are initially far from each other. This trend makes physical sense because the screening effect associated with salt ions plays a significant role only at long range. At short distances (compared to the size of solvent), electrostatic screening is not expected to be important. For example, the computational study of Elcock and co-workers (*17*) of the association of acetate and methylammonium (model compounds for salt bridges) found that the free energy minimum that corresponds to the dehydrated salt bridge state is not diminished even up to 2 M salt. As the salt concentration increases from 0 to 0.3 M (similar to the high-salt condition here), the stability of the dehydrated salt bridge is reduced by only 0.2 kcal/mol.

These analyses suggest that even at 350 mM KCl, a significant fraction of salt bridges in the unbound form of IHF is expected to be stable (8 of 17 residues have P_{salt} values of >0.1 in at least one 25−50 ns trajectory). This conclusion seems to be inconsistent with the proposal of Record and co-workers that salt bridges are unstable at 350 mM K^+ and hence that there is no disruption of salt bridges coupled to DNA binding. This second hypothesis was proposed to explain the experimental observation that $\Delta H^\circ_{\text{sp}}$ for specific binding increases (becomes less negative) significantly from −56.1 kcal/mol at 60 mM K^+ to −10.8 kcal/mol at 350 mM K^+ at 40 °C. More recent analyses (*18*), however, found that a significant portion of the strong salt dependence is due to the Hofmeister effect associated with Cl^-; extrapolations of results in different salt solutions (KCl, KF, and KGlu) showed that, at low

Table 2: r_{init}, $P_{\text{no-salt}}$, and P_{salt} Values for the 19 Other Cationic Residues[a]

residue	r_{init} (Å)	$P_{\text{no-salt}}$	P_{salt}	residue	r_{init} (Å)	$P_{\text{no-salt}}$	P_{salt}
K5α	3.0	0.87	0.97	R9β	2.9	0.76	0.96
		0.99/0.96	1.00/0.99			0.97/0.97	0.94/0.91
K15α	4.6	0.86	0.92	K20β	3.0	0.03	0.06
		0.96/0.91	0.89/0.86			0.02/0.15	0.04/0.02
R21α	5.4	0.43	0.54	R42β	3.0	0.76	0.88
		0.66/0.43	0.58/0.31			0.70/0.52	0.32/0.24
R35α	2.9	1.00	1.00	R46β	3.0	0.28	0.34
		1.00/1.00	1.00/1.00			0.11/0.25	0.39/0.21
R36α	3.3	0.88	0.65	R62β	6.7	0.00	0.39
		0.79/0.79	1.00/0.81			0.00/0.00	0.00/0.00
K66α	12.4	0.08	0.00	K65β	10.1	0.00	0.00
		0.00/0.00	0.00/0.00			0.00/0.00	0.00/0.00
R77α	3.6	0.83	0.94	K69β	6.6	0.36	0.26
		0.81/0.58	0.89/0.96			0.32/0.51	0.14/0.20
K86α	7.2	0.02	0.05	K84β	3.0	0.70	0.31
		0.10/0.02	0.14/0.00			0.40/0.81	0.26/0.25
R90α	3.0	1.00	1.00	R89β	2.8	0.99	1.00
		0.98/0.99	1.00/1.00			0.95/1.00	1.00/1.00
K97α	4.5	0.55	0.56				
		0.46/0.57	0.56/0.42				

[a]See footnote of Table 1.

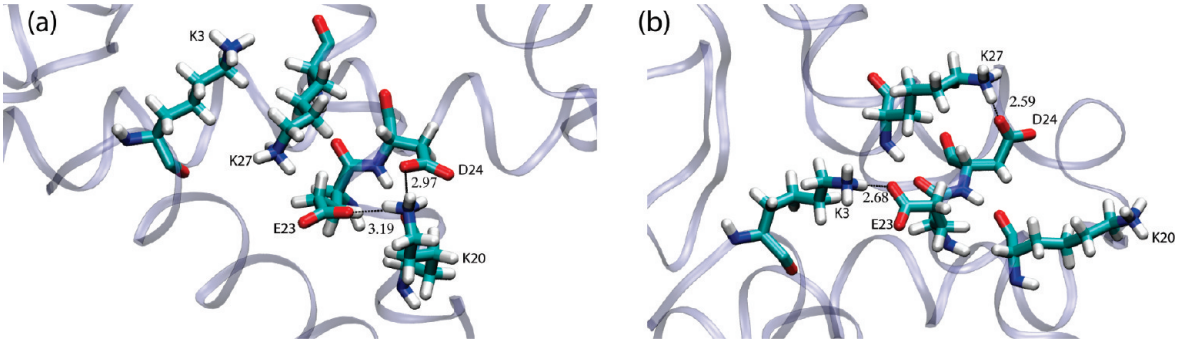

FIGURE 6: Positions of K3, K20, E23, D24, and K27 on the β subunit in (a) the IHF conformation in the IHF−DNA complex [PDB entry 1IHF (*8*)] and (b) a snapshot at 22.4 ns from the no-salt simulation. The five charged residues are shown as licorice, while the protein is shown as ribbons. The salt bridge distances ($r_{\text{min-NO}}$, in angstroms) for salt bridges are also shown. Comparison between panels a and b indicates that the salt bridge pattern involving K20β changes during the simulation.

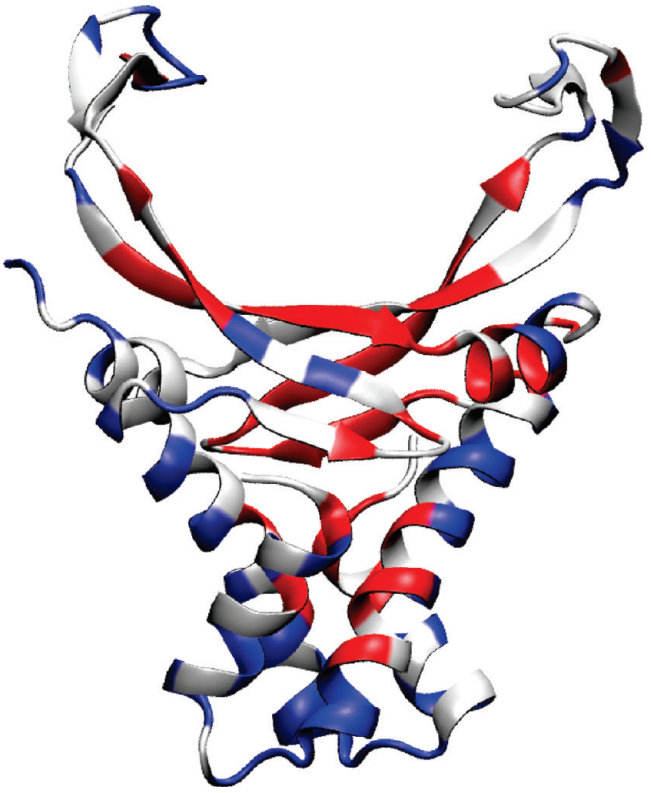

FIGURE 7: Differential residue-averaged electrostatic potential ($\Delta\phi_{res}$) between the simulated apo structure and the crystal apo structure, mapped onto the crystal apo structure. $\Delta\phi_{res}$ is larger than 5 kcal mol^{-1} e^{-1}, less than -5 kcal mol^{-1} e^{-1}, and between -5 and 5 kcal mol^{-1} e^{-1} for the blue, red, and white regions, respectively.

salt concentrations, the binding enthalpy is essentially independent of the salt concentration. Nevertheless, it is of interest to discuss other factors that can potentially contribute to the salt dependence of binding thermodynamics in light of the current simulations. For example, because our simulation results indicate that the disruption of multiple salt bridges is still likely involved in DNA binding at even 350 mM K^+, we suspect that the increase in ΔH°_{sp} is due, at least in part, to the increase in the enthalpy change of disruption of a salt bridge (ΔH_d) with respect to the increase in K^+ concentration. This can be understood by comparing the processes of salt bridge disruption under no-salt and high-salt conditions. The enthalpy change for salt bridge disruption under the no-salt condition ($\Delta H_d^{no\text{-}salt}$) is negative (*44*) because of the increase in hydration enthalpy when two charged species are separated. At higher salt concentrations, however, the disruption of a salt bridge is coupled to the formation of two side chain−counterion interaction pairs. As a result, the enthalpy change (ΔH_d^{salt}) should be $\Delta H_d^{no\text{-}salt}$ plus the enthalpy change for formation of two side chain−counterion pairs, which is positive, and therefore, ΔH_d^{salt} should be larger (less negative) than $\Delta H_d^{no\text{-}salt}$; at a qualitative level, this effect is embedded with the calculations for the enthalpy change for K^+−Cl^- ion pair dissociation at different concentrations (see the Supporting Information). Whether this effect is important on a quantitative scale remains to be determined because the estimated impact of K^+−Cl^- ion pair dissociation is fairly modest in magnitude (see the Supporting Information); moreover, this contribution can be offset by similar effects, but of the opposite sign, associated with the formation of ionic interactions between the cationic residues in IHF and phosphoryl groups in DNA.

Impact on the Prediction of DNA Binding Sites. As mentioned in the introductory section, an important goal of this study is to explore how sampling salt bridge dynamics impacts the prediction of DNA binding sites on proteins. The goal is motivated by the consideration that salt bridge formation or disruption is expected to significantly modulate the system electrostatics, which play a major role in many DNA binding site prediction algorithms (*39*−*41*, *45*−*47*). Indeed, many such algorithms have been tested or trained using the structures of protein−DNA complexes (with the DNA excised). If there is a significant structural difference between the unbound and bound conformations of the protein, such as the formation or disruption of a large number of salt bridges, the electrostatic properties may differ significantly. As a result, an algorithm trained using bound state structures may not be effective because realistic applications will require using the unbound state as input.

To illustrate the change of surface electrostatic potential in IHF due to salt bridge dynamics, we calculate the differential electrostatic potential between IHF adopting the conformation in the IHF−DNA complex [PDB entry 1IHF (*8*)] and a snapshot from the no-salt simulation in which the maximum number (12 of 17) of binding-site cationic residues have formed salt bridges (see Figure 7). For the red regions in Figure 7, the residue-averaged electrostatic potential difference ($\Delta\phi_{res}$) is more than 5 kcal mol^{-1} e^{-1}; $\Delta\phi_{res}$ is less than 5 kcal mol^{-1} e^{-1} for the blue regions, whereas it is between -5 and 5 kcal mol^{-1} e^{-1} for the white regions. It is clear that for most of the DNA binding interface, the electrostatic potential is decreased by more than 5 kcal mol^{-1} e^{-1} as the IHF structure relaxes away from the conformation in the IHF−DNA complex. We emphasize here that the structural variations sampled in this study are limited to the time scale of 25−50 ns; with the realistic structure of apo state IHF, the difference in the structural and electrostatic properties can be even greater.

The key question is whether such a change in the surface electrostatic potential has a significant impact on the performance of structure-based algorithms for DNA binding site prediction. As discussed in Computational Methods, we tested this using two popular structure-based web servers. The first server was patch plus finder (PPF) (*39*), which finds the largest continuous patch with positive electrostatic potential on the protein surface (*47*). Using the IHF structure in the IHF−DNA complex as input, the predicted patch by PPF (see Figure 8a) contained 63 residues and coincided with the authentic DNA binding interface. Using the snapshot with altered salt bridge patterns as the input structure, however, the predicted patch (see Figure 8b) contained 35 residues and spanned only half of the arm domain.

The second server we tested was Preds (*40*, *41*), which makes prediction on the basis of not only surface electrostatic potential but also molecular shape features. An output of Preds is a statistical score, P_{score}, and the input protein is predicted to be a DNA binding protein if P_{score} is higher than 0.12. Using the IHF structure in the IHF−DNA complex as input, the predicted P_{score} was 0.27; the score became substantially lower (0.17) when the snapshot from the simulation was used. Another output of Preds is the predicted binding sites, which are shown in panels c and d of Figure 8 with different IHF structures as input; the difference is relatively small, and the predicted binding site is reduced from 90 to 73 residues when the snapshot from MD simulation is used instead of the IHF structure in the IHF−DNA complex. Therefore, the prediction of DNA binding site appears

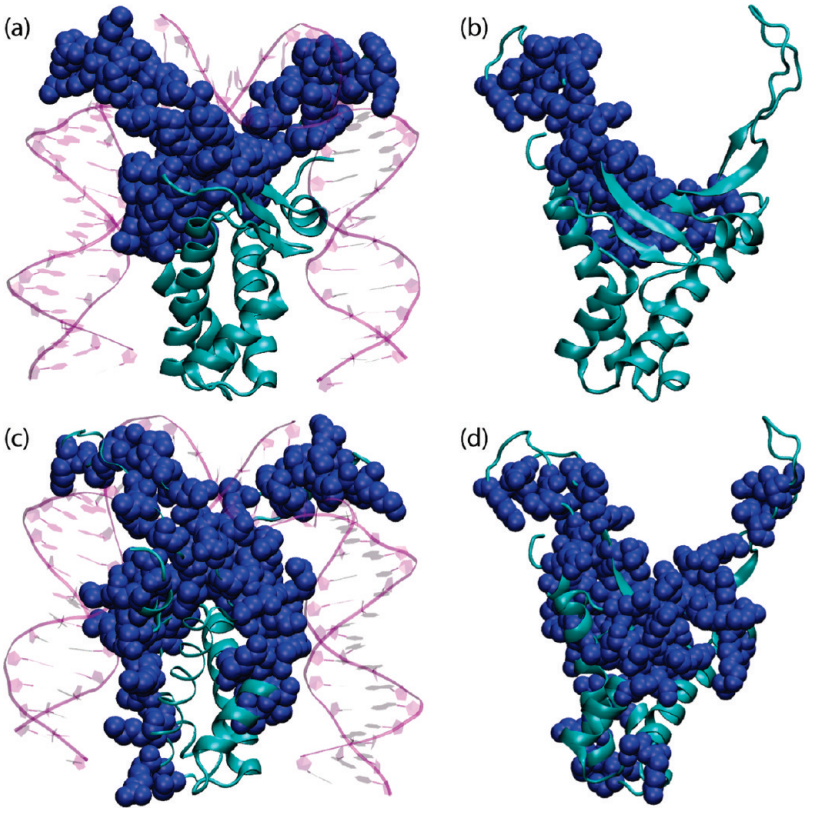

FIGURE 8: Results of DNA binding site prediction using two popular online servers. IHF is shown as a cartoon, and the residues predicted for the binding sites are colored blue in a van der Waals scheme. (a and b) DNA binding sites predicted by PPF for the (a) crystal apo and (b) simulated unbound IHF structures. (c and d) DNA binding sites predicted by Preds for (c) the crystal apo structure and (d) the simulated unbound structure.

to be more robust when electrostatic properties are augmented by geometrical considerations.

CONCLUDING REMARKS

Protein−DNA binding processes likely involve many structural transitions at both domain and side chain levels, which are not be straightforward to capture using experiments alone. In this study, motivated by the proposal of Record and co-workers in recent thermodynamic studies of specific DNA binding to IHF (*9*), we have focused on the behavior of charged residues in IHF using explicit solvent molecular dynamics simulations. Even at the somewhat limited time scale of 25−50 ns, we have observed rather rich behaviors. Of the 17 cationic residues noted by Record and co-workers, most are engaged in salt bridge interactions for a significant portion of the trajectories, especially under the no-salt condition. This observation suggests that, from a structural point of view, their proposal that IHF−DNA binding is coupled with the disruption of preexisting salt bridges in apo IHF is plausible. However, switching of salt bridge pairs, i.e., the simultaneous disruption and formation of salt bridges, that involve nonbinding site cationic residues has also been observed during the MD simulations. Therefore, the unusual thermodynamic characteristics of IHF−DNA binding likely arise from the interplay between fairly complex dynamics of charged residues both in and beyond the DNA binding site. With regard to the salt effect, the MD simulations suggest that it contributes to the screening of electrostatic interactions only when salt bridge pairs are far from each other, consistent with a recent computational study of small molecules that form salt bridges (*17*). Therefore, the large dependence of the IHF−DNA binding enthalpy on salt concentration may not be due to a significant decrease in the number of stable salt bridges in apo IHF at high salt concentrations; this is qualitatively consistent with more recent analysis (*18*), which found that the salt dependence of binding enthalpy is largely a Hofmeister effect.

Our simulation study further highlights that the electrostatic properties of DNA-binding proteins can be rather different in the apo and DNA-bound states. This has important implications for the design of methods for predicting DNA binding sites in proteins. As we have illustrated using two examples, it appears to be essential either to explicitly consider sampling salt bridge dynamics when evaluating electrostatic properties or to supplement electrostatic properties with geometrical criteria based on structural complementarity.

ACKNOWLEDGMENT

We acknowledge Professor Tom Record for encouraging us to examine the problem and for stimulating discussions. Computational resources from the National Center for Supercomputing Applications at the University of Illinois and the Center for High Throughput Computing (CHTC) at the University of Wisconsin are greatly appreciated.

SUPPORTING INFORMATION AVAILABLE

Dependence of salt bridge interactions on salt concentration with a KCl solution as an example and time dependence of salt bridge distances for all 36 cationic residues during MD simulations under no-salt and high-salt conditions. This material is available free of charge via the Internet at http://pubs.acs.org.

REFERENCES

1. Alberts, B., Bray, D., Lewis, J., Raff, M., Roberts, K., and Watson, J. D. (1994) Molecular biology of the cell, Garland Publishing, Inc., New York.
2. McHenry, C. S. (1988) DNA polymerase-III holoenzyme of *Escherichia coli*. *Annu. Rev. Biochem. 57*, 519–550.
3. Bewley, C. A., Gronenborn, A. M., and Clore, G. M. (1998) Minor groove-binding architectural proteins: Structure, function, and DNA recognition. *Annu. Rev. Biophys. Biomol. Struct. 27*, 105–131.
4. Rice, P. A. (1997) Making DNA do a U-turn: IHF and related proteins. *Curr. Opin. Struct. Biol. 7*, 86–93.
5. Swinger, K. K., and Rice, P. A. (2004) IHF and HU: Flexible architects of bent DNA. *Curr. Opin. Struct. Biol. 14*, 28–35.
6. Williams, L. D. (2000) Electrostatic mechanisms of DNA deformation. *Annu. Rev. Biophys. Biomol. Struct. 29*, 497–521.
7. Ma, L., Yethiraj, A., Chen, X., and Cui, Q. (2009) A computational framework for mechanical response of macromolecules: Application to the salt concentration dependence of DNA bendability. *Biophys. J. 96*, 3543–3554.
8. Rice, P. A., Yang, S. W., Mizuuchi, K., and Nash, H. A. (1996) Crystal structure of an IHF-DNA complex: A protein-induced DNA U-turn. *Cell 87*, 1295–1306.
9. Holbrook, J. A., Tsodikov, O. V., Saecker, R. M., and Record, M. T., Jr. (2001) Specific and non-specific interactions of integration host factor with DNA: Thermodynamic evidence for disruption of multiple IHF surface salt-bridges coupled to DNA binding. *J. Mol. Biol. 310*, 379–401.
10. Nadassy, K., Wodak, S. J., and Janin, J. (1999) Structural features of protein-nucleic acid recognition sites. *Biochemistry 38*, 1999–2017.
11. Perl, D., Mueller, U., Heinemann, U., and Schmid, F. X. (2000) Two exposed amino acid residues confer thermostability on a cold shock protein. *Nat. Struct. Biol. 7*, 380–383.
12. Saecker, R. M., and Record, M. T., Jr. (2002) Protein surface salt bridges and paths for DNA wrapping. *Curr. Opin. Struct. Biol. 12*, 311–319.
13. Grove, A., and Saavedra, T. C. (2002) The role of surface-exposed lysines in wrapping DNA about the bacterial histone-like protein HU. *Biochemistry 41*, 7597–7603.
14. Grove, A. (2003) Surface salt bridges modulate DNA wrapping by the type II DNA-binding protein TF1. *Biochemistry 42*, 8739–8747.
15. Daopin, S., Sauer, U., Nicholson, H., and Matthews, B. W. (1991) Contributions of engineered surface salt bridges to the stability of t4 lysozyme determined by directed mutagenesis. *Biochemistry 30*, 7142–7153.
16. Strop, P., and Mayo, S. L. (2000) Contribution of surface salt bridges to protein stability. *Biochemistry 39*, 1251–1255.
17. Thomas, A. S., and Elcock, A. H. (2006) Direct observation of salt effects on molecular interactions through explicit-solvent molecular dynamics simulations: Differential effects on electrostatic and hydrophobic interactions and comparisons to poisson-boltzmann theory *J. Am. Chem. Soc. 128*, 7796–7806.
18. Meulen, K. A. V., Saecker, R. M., and Record, M. T., Jr. (2008) Formation of a wrapped DNA-protein interface: Experimental characterization and analysis of the large contributions of ions and water to the thermodynamics of binding IHF to H′ DNA. *J. Mol. Biol. 377*, 9–27.
19. Lindahl, E., Hess, B., and van der Spoel, D. (2001) Gromacs 3.0: A package for molecular simulation and trajectory analysis. *J. Mol. Model. 7*, 306–317.
20. Berendsen, H. J. C., Vanderspoel, D., and Vandrunen, R. (1995) Gromacs: A message-passing parallel molecular-dynamics implementation. *Comput. Phys. Commun. 91*, 43–56.
21. Jorgensen, W. L., and Tiradorives, J. (1988) The OPLS potential functions for proteins: Energy minimizations for crystals of cyclicpeptides and crambin. *J. Am. Chem. Soc. 110*, 1657–1666.
22. Jorgensen, W. L., Chandrasekhar, J., Madura, J. D., Impey, R. W., and Klein, M. L. (1983) Comparison of simple potential functions for simulating liquid water. *J. Chem. Phys. 79*, 926–935.
23. Essmann, U., Perera, L., Berkowitz, M. L., Darden, T., Lee, H., and Pedersen, L. G. (1995) A smooth particle mesh ewald method. *J. Chem. Phys. 103*, 8577–8593.
24. Steinbach, P. J., and Brooks, B. R. (1994) New spherical-cutoff methods for long-range forces in macromolecular simulation. *J. Comput. Chem. 15*, 667–683.
25. Miyamoto, S., and Kollman, P. A. (1992) Settle: An analytical version of the shake and rattle algorithm for rigid water models. *J. Comput. Chem. 13*, 952–962.
26. Ryckaert, J. P., Ciccotti, G., and Berendsen, H. J. C. (1977) Numerical-integration of cartesian equations of motion of a system with constraints: Molecular-dynamics of *n*-alkanes. *J. Comput. Phys. 23*, 327–341.
27. Nose, S. (1984) A unified formulation of the constant temperature molecular-dynamics methods. *J. Chem. Phys. 81*, 511–519.
28. Hoover, W. G. (1985) Canonical dynamics: Equilibrium phase-space distributions. *Phys. Rev. A 31*, 1695–1697.
29. Berendsen, H. J. C., Postma, J. P. M., Vangunsteren, W. F., Dinola, A., and Haak, J. R. (1984) Molecular dynamics with coupling to an external bath. *J. Chem. Phys. 81*, 3684–3690.
30. Gunner, M. R., Mao, J., Song, Y., and Kim, J. (2006) Factors influencing the energetics of electron and proton transfers in proteins. What can be learned from calculations? *Biochim. Biophys. Acta 1757*, 942–968.
31. Li, H., Robertson, A. D., and Jensen, J. H. (2005) Very fast empirical prediction and interpretation of protein pK_a values. *Proteins: Struct., Funct., Bioinf. 61*, 704–721.
32. Bas, D. C., Rogers, D. M., and Jensen, J. H. (2008) Very fast prediction and rationalization of pK_a values for protein-ligand complexes. *Proteins: Struct., Funct., Bioinf. 73*, 765–783.
33. Leontyev, I. V., and Stuchebrukhov, A. A. (2010) Electronic continuum model for molecular dynamics simulations of biological molecules. *J. Chem. Theory Comput. 6*, 1498–1508.
34. Harder, E., MacKerell, A. D., Jr., and Roux, B. (2009) Many-body polarization effects and the membrane dipole potential. *J. Am. Chem. Soc. 131*, 2760–2761.
35. Jiao, D., Golubkov, P. A., Darden, T. A., and Ren, P. (2008) Calculation of protein-ligand binding free energy by using a polarizable potential. *Proc. Natl. Acad. Sci. U.S.A. 105*, 6290–6295.
36. Brooks, B. R., Bruccoleri, R. E., Olafson, B. D., States, D. J., Swaminathan, S., and Karplus, M. (1983) CHARMM: A program for macromolecular energy, minimization, and dynamics calculations *J. Comput. Chem. 4*, 187–217.
37. Nina, M., Im, W., and Roux, B. (1999) Optimized atomic radii for protein continuum electrostatics solvation forces. *Biophys. Chem. 78*, 89–96.
38. MacKerell, A. D., Bashford, D., Bellott, M., Dunbrack, R. L., Evanseck, J. D., Field, M. J., Fischer, S., Gao, J., Guo, H., Ha, S., Joseph-McCarthy, D., Kuchnir, L., Kuczera, K., Lau, F. T. K., Mattos, C., Michnick, S., Ngo, T., Nguyen, D. T., Prodhom, B., Reiher, W. E., Roux, B., Schlenkrich, M., Smith, J. C., Stote, R., Straub, J., Watanabe, M., Wiorkiewicz-Kuczera, J., Yin, D., and Karplus, M. (1998) All-atom empirical potential for molecular modeling and dynamics studies of proteins. *J. Phys. Chem. B 102*, 3586–3616.
39. Shazman, S., Celniker, G., Haber, O., Glaser, F., and Mandel-Gutfreund, Y. (2007) Patch Finder Plus (PFplus): A web server for extracting and displaying positive electrostatic patches on protein surfaces. *Nucleic Acids Res. 35*, W526–W530.
40. Tsuchiya, Y., Kinoshita, K., and Nakamura, H. (2005) PreDs: A server for predicting dsDNA-binding site on protein molecular surfaces. *Bioinformatics 21*, 1721–1723.
41. Tsuchiya, Y., Kinoshita, K., and Nakamura, H. (2004) Structure-based prediction of DNA-binding sites on proteins using the empirical preference of electrostatic potential and the shape of molecular surfaces. *Proteins: Struct., Funct., Bioinf. 55*, 885–894.
42. Spolar, R. S., and Record, M. T., Jr. (1994) Coupling of local folding to site-specific binding of proteins to DNA. *Science 263*, 777–784.
43. Barlow, D. J., and Thornton, J. M. (1983) Ion-pairs in proteins. *J. Mol. Biol. 168*, 867–885.
44. Kauzmann, W. (1959) Some factors in interpretation of protein denaturation. *Adv. Protein Chem. 14*, 1–57.
45. Gou, Z., Hwang, S., and Kuznetsov, B. I. (2006) Sequence-based prediction of DNA-binding sites on DNA-binding proteins. Proceedings of the Fifth International Conference on Bioinformatics of Genome Regulation and Structure, Vol. 1, pp 268−271.
46. Tjong, H., and Zhou, H. X. (2007) DISPLAR: An accurate method for predicting DNA-binding sites on protein surfaces. *Nucleic Acids Res. 35*, 1465–1477.
47. Stawiski, E. W., Gregoret, L. M., and Mandel-Gutfreund, Y. (2003) Annotating nucleic acid-binding function based on protein structure. *J. Mol. Biol. 326*, 1065–1079.
48. Humphrey, W., Dalke, A., and Schulten, K. (1996) VMD: Visual Molecular Dynamics. *J. Mol. Graphics 14*, 33–38.